



# Numerical Investigation of Dynamic Stress Distribution in a Railway Embankment Reinforced by Geogrid Based Weak Soil Formation Using Hybrid RNN-EHO

M. A. Balasubramani<sup>(✉)</sup>, R. Venkatakrishnaiah, and K. V. B. Raju

Department of Civil Engineering, Bharath Institute of Higher Education and Research, Chennai, India

mabalacivil@gmail.com, Venkatakrishnaiah.civil@bharathuniv.ac.in

**Abstract.** As the primary method of track support, traditional sloping embankments are typically used by railroad lines. Geosynthetically Reinforced Soil (GRS) systems, as an alternative to traditional embankments, have gained appeal, notably for high-speed lines in India. This system's reduced base area compared to traditional embankments means that less ground stabilisation, improvement, and land taking is necessary. The research's findings provide intriguing strategies that may be implemented into the way tracks are designed now to accommodate faster freight trains pulling greater loads. This research explains how to anticipate the bearing capacity of weak sand supported by a method of compacted granular fill over natural clay soil using a hybrid Recurrent Neural Network (RNN) and Elephant Herding Optimization (EHO) with Geogrid reinforced soil foundation. The exact prediction target for the proposed model was developed by using displacement amplitude as an output index. A number of elements influencing the foundation bed's properties, Geogrid reinforcement, and dynamic excitation have been taken into account as input variables. The RNN-anticipated EHO's accuracy was compared to that of three other popular approaches, including ANN, HHO, CFA, and MOA. Strict statistical criteria and a multi-criteria approach were principally used to assess the predictive power of the developed models. The model is also examined using fresh, independent data that wasn't part of the initial dataset. The hybrid RNN-EHO model performed better in predicting the displacement amplitude of footing laying on Geogrid-reinforced beds than the other benchmark models. Last but not least, the sensitivity analysis was used to highlight how input parameters might affect the estimate of displacement amplitude.

**Keywords:** Recurrent Neural Network (RNN) · Elephant Herding Optimization (EHO) · Geogrid · Settlement · Soil reinforcement · Weak Sand · Mayfly optimization algorithm · Jellyfish search algorithm · Cuttlefish algorithm and artificial neural network

## 1 Introduction

High-speed train track and ground responses are primarily influenced by the interplay of train loads and Rayleigh surface waves on the railway embankment and track bed [1–3]. One of the most crucial elements in explaining, forecasting, or predicting a track reaction and considering the proper remedial action is the bed's Rayleigh wave velocity. Studies have demonstrated the requirement for safety on soft ground railroads due to the high-speed trains' extensive range of vibration, particularly while operating at critical speed. The inherent vibrating characteristics of the rail systems define this speed. The important speed is the train speed that induces a pseudo-resonance event in the bed and is roughly equal to or larger than the Rayleigh wave speed of the bed [4, 5]. The critical speed also leads to significant track deviations, severe embankment vibration, and cone-shaped ground wave motion. The processes for bed soil augmentation are influenced by a number of variables, including train speed, soil type, embankment height, and the thickness of soft and loose sediments. Numerous methods, including geosynthetics (geogrid), vibro-replacement with stone columns, dry deep soil mixing (cement columns), concrete piles with or without integrated caps, removal replacement methods with suitable materials, and the installation of mechanical reinforcements like plate anchors and helical piles, can be used to improve the soils beneath railway embankments [6, 7].

While geogrid reinforcement has long been employed in other geotechnical applications, there hasn't been much research on how it may be applied in railway engineering. This could be the case since there isn't a design procedure especially for railway embankments and the industry is cautious [8]. Although it has been shown that the reinforcement improves performance under static and cyclic loads, little is known about where the geogrid works best and how it performs in difficult conditions like railway gravel. Additional knowledge of how ballast and geogrid behave in a railway application may aid in the advancement of useful design techniques. In terms of cost and the environment, such an application may have an effect on future train design and track restoration [9]. To sustain the repeated stress caused by train passes, ballast acts as a foundation to absorb energy, drain easily, and withstand pressures acting both vertically and laterally (Selig and Waters). However, significant technological issues [10] make it difficult to carry out these important duties. Train loading forces may cause ballast to be rearranged and degraded during several loading cycles, diminishing grain interlocking and allowing lateral particle migration. As ballast particles migrate laterally, track stability may suffer as a result of a reduction in frictional strength. Loss of track geometry results from vertical and lateral deformations brought on by spreading or foundation issues. Maintaining the ballasted foundation's shape is essential since track maintenance due to geotechnical issues is more costly than other track expenditures.

Numerous studies have focused at ways to improve the bearing capacity of shallow foundations as well as how to produce construction materials like concrete and geopolymer bricks from waste resources. Ziegler *et al.* [11]'s comparison of the reinforced case with the unreinforced one under the same load revealed an improvement in bearing capacity and a discernible reduction in indisplacements. These results were shown to be caused by the geogrid reinforcement's limiting effect and interlocking mechanism, which convert the reinforced case's more or less straight deviatoric stress route into an isotropic stress path. Ballasted railway track samples that had been exposed to

mixed vertical-horizontal cyclic stresses experienced settlement at high relative train speeds, according to Yu *et al.* [12]. At the ballast-subballast contact, the subballast-subgrade interface, and the effect of subgrade stiffness on geogrid performance at the subballast-subgrade interface, we looked at the performance advantages of installing geogrid. Using laboratory testing and finite element modeling, Esmaeili *et al.* [13] have shown how geogrid affects the stability and settlement of high railway embankments. To achieve this, the crest of a loading chamber with dimensions of 240 x 235 x 220 cm was covered with five sets of 50 cm-high embankments created at a scale of 1:20. The original embankments weren't strengthened with geogrid layers. In order to lessen the persistence of train-induced deformation, Zhang *et al.* [14] developed a ground rehabilitation strategy that includes continual permeation grouting injections into the bearing strata of the group piles. The consequences of the suggested mitigation strategy were then investigated using numerical simulations based on complex constitutive models and soil-water linked finite element-finite difference (FE)-(FD) compound arithmetic. Recycled concrete aggregates and geosynthetics may improve the performance of ballasted railway tracks, according to study by Punetha *et al.* [15]. Employing two-dimensional finite element analysis, the value of using geogrids, geocells, and recycled concrete aggregates in the ballasted railway tracks is examined. Effectiveness is assessed using the track settlement. The results show that using recycled aggregates and geosynthetics significantly lowers track settlement and could enable greater train speeds at the same allowable settlement level. Understanding the operation of the geogrid material layers used to reinforce high railway embankments is the major goal of this investigation. The study focuses on two elements that impact the serviceability of railway embankments: reducing crest settling and preventing sliding in the embankment body. The results of all reinforced numerical models and preliminary numerical modeling were taken into account to determine the appropriate level for installing the geogrid layers. This was accomplished by adding one to four layers of geogrid to each of the second through fifth set of embankments to strengthen them. No additional geogrid reinforcement was used while building the original sequence of embankments.

## 2 Proposed Methodology

### 2.1 Model Clay Barrier's Compositional Characteristics

Sand and kaolin were combined in a 4:1 dry weight ratio, much as the soil in the current experiment, to imitate the clay barrier and attain the required hydraulic conductivity of 109 m/s. The model clay barrier material was determined to have a maximum dry unit weight of 15.9 kN/m<sup>3</sup>, a liquid limit of 38%, a plastic limit of 16%, a coefficient of permeability of 0.4 109 m/s, and an ideal moisture content of 22% (standard Proctor compaction test). The Unified Soil Classification System (UCSC), which classifies the chosen combination as a CL type, was found to have qualities that are equivalent to those of the bulk of locally accessible organically generated clays in most of India. Additionally, it illustrates the clay barriers used in landfills' fine-grained soil bandwidth features [16]. When wet compacted at OMC + 5%, it was discovered that the clay barrier had a comparable dry unit weight and shear strength of between 30 and 40 kN/m<sup>2</sup>.

## 2.2 Geogrid

Bi-directional geogrids are used throughout all series of experiments. Table 1 displays the geogrid's characteristics utilised in this investigation.

**Table 1.** Geogrid index characteristics

Parameter	Value
Thickness (mm)	1.8
Mass per unit area (Kg/m <sup>2</sup> )	0.532
Ultimate tensile strength (kN/m)	7.6
Aperture size (mm)	23

## 2.3 Measuring Subgrade Stiffness

The stiffness and strength characteristics of the subgrade and formation were evaluated at various testing phases (the formation layer was replaced prior to each test). Unrestricted compression tests were used to measure strength, and a circular plate load test was used to measure stiffness under the Losenhausen piston. These figures were contrasted with studies utilizing pocket penetrometers, dynamic penetration tests, and light falling deflectometers [17]. The plate load test stiffness results were thought to be the most trustworthy, and the Young's modulus was calculated using:

$$S_{pit} = \frac{2P(1 - PR^2)}{\pi r \mu} \quad (1)$$

The plate applied load is  $P$ , Poisson's ratio is  $PR$  and  $\mu$  plate deflection is all present and the plate's radius is  $r$  located. In order to prevent problems with early setup  $S_{pit}$ , the phrase is used to describe the tangent Young's modulus computed from the first half of the second load cycle curve (i.e. plate-surface contact errors).

Although a track settling analysis is provided, the approach used here employs the route restriction ( $t$ ) given by:

$$t = \frac{S_{pit}}{P} = \frac{S_{riff}}{P_{press}} \quad (2)$$

The relevant unreinforced ballast control tests in this research are designated as CT<sub>1</sub>, CT<sub>2</sub>, and CT<sub>3</sub>, along with details regarding the testing. The consistency of the tests was shown by the fact that the predicted resilient modulus values at the breakpoint stress for each test often followed the same pattern as the measured plate load  $S_{pit}(t)$  modulus values.

### 2.4 Multi Objective Function

The bad sand’s stability is improved in this step using the optimization parameter of the hybrid RNN-EHO method, which is also employed to improve the appearance of the proposed Geogrid. The main goal of the suggested hybrid RNN-EHO approach in this case is to reduce the form characteristic, which is scientifically unique in Eq. (3),

$$OF = Min_E(\delta_P, \delta_{bc}, \delta_s) \tag{3}$$

where,  $\delta_s$  are the pressure and bearing capacity error minimizations and the pressure and  $\delta_P, \delta_{bc}$  are bearing capacity error minimizations of the weak soil formation.

### 2.5 Improving Settlement-Based Geogrid using Hybrid RNN-EHO Technique

Use RNN to choose the most appropriate subset of dataset attributes in this case to discriminate between susceptible and regular data. RNN mimics the creation of goal functions and feature selection. According to the same theory, an RNN enhances the answer by progressively choosing the best options while removing the less desirable ones [18]. Figure 1 shows the RNN model’s architectural layout. The input layer is made up of vectors that  $x, y(t), z(t)$  and  $w(t - 1)$  respectively, correspond to the present user, item, response action, and hidden layer state. The user  $m$  is referenced in the model via  $l * 1$  a vector, where  $m^{th}$  element is 1 and the remaining elements are 0. An  $n * 1$  or  $1 * 1$  vector refers to each item (or kind of feedback action) in the same manner.  $H$  and  $m$  stand for the user’s and the item’s respective hidden layers. The hidden layer’s output  $w$  at the current period stage  $t$  is referenced by the vector  $w(t)$ .  $O$  is the layer of output.

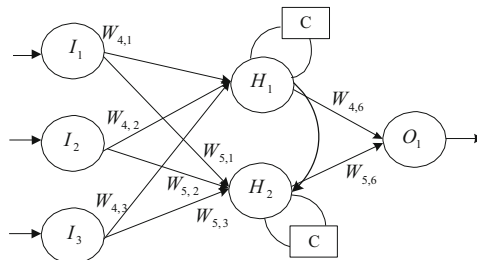


**Fig. 1.** The architecture of the RNN model

Through the weight matrix  $A$  the user vector  $x$  from the input layer is linked to the hidden layer  $H$ . This portion is non-recurring, and equation is used to compute the hidden layer’s output (4),

$$H = f(Ax) \tag{4}$$

The dimension of the concealed layer  $H$  is represented by the vector  $D * 1$  in this area.  $A$  is a  $D * m$  matrix with a user’s choice referred to in each column. The equation provides the sigma function  $f$  as the Eq. (5).

$$f(x) = \frac{1}{1 + e^{-x}} \tag{5}$$

The weight matrices  $M$ ,  $N$  and  $L$  respectively, link the input layer's vectors and to the hidden layer's vectors  $x$ ,  $y(t)$ ,  $z(t)$  and  $w(t - 1)$ . The hidden layer records  $s(t - 1)$  prior user behaviour while this section of the model is repeated. To determine the hidden layer's output at the time stamp,  $t$ ,  $w(t)$  apply Eq. (6).

$$w(t) = f(Mx(t) + Ny(t) + Lw(t - 1)) \tag{6}$$

where,  $D * 1$  a vector is  $w(t)$ .  $M$ ,  $N$  and  $L$  are  $DXn$ ,  $DX1$  and  $DXD$  are the corresponding matrices  $M$ . The feature of an item is referenced in each column of the matrix  $N$ . Additionally, each column in the matrix denotes a certain kind of feedback activity. A vector  $nX1$  is produced by the system at the period imprint and  $t$ ,  $O(t)$  is computed using Eq. (7),

$$O(t) = g(Ys(t) + Zh) \tag{7}$$

The weight matrices for the hidden layer and the output layer are  $Y$  and  $Z$ . The equation provides the softmax function as  $g$ .

$$g(x) = \frac{e^x}{\sum_{i=1}^k e^{x_i}} \tag{8}$$

The assessment of the likelihood that the user  $m$  would approach the item  $j$  at the following timestamp provided by the historical feedback that is calculated using Eq. (9)  $O_j(t + 1)$  is the output element  $j^{\text{th}}$  after the network has been trained.

$$O_j(t + 1) = P(v_j(t + 1) = 1/x, y(t), z(t), w(t - 1)) \tag{9}$$

When a proposal is executed, the output at the model's final time stamp is determined for each user. Simply choose the  $P$  output's largest items, and it is advisable to use their indexes. The Geogrid controller is then given the RNN as input based on the weak soil development in the railway track.

### 2.6 The Procedure of the EHO in Realizing the Learning of RNN

The learning function of the RNN algorithm is implemented by the EHO algorithm. The programme was inspired by the herding behaviour of elephants. Due to the gregarious character of the elephant, there are several factions of female elephants in the group, each of which is carrying a calf [19]. Each group's movement is influenced by its matriarch or leader elephant. As seen in Fig. 2, the Female Elephant (FE) once lived with family gatherings while the Male Elephant (ME) grew up and lives alone while maintaining contact with his family group.

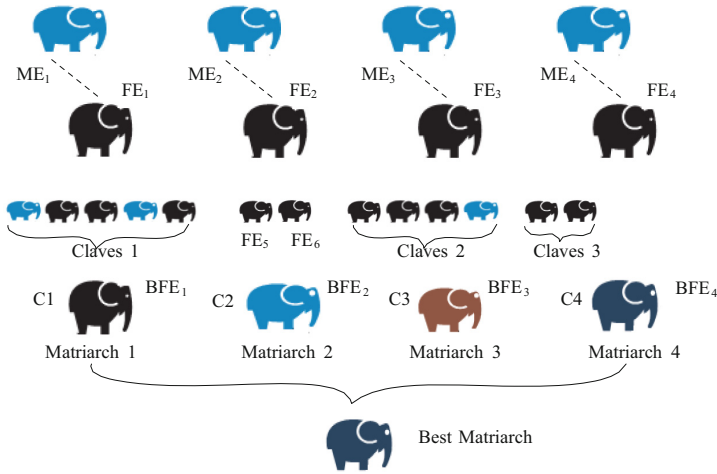


Fig. 2. EHO elephants' behaviours

The following assumptions about herding are taken into consideration in EHO:

- The total elephant population is divided into clans, with each clan containing a specified number of elephants.
- A established population of ME permits their clan and life to be left alone.
- A matriarch oversees the operations of each tribe.

One can infer that there are the same number of elephants in each clan. The matriarchal group in the elephant herd is organised in the greatest way possible, whereas the male elephant herd is positioned in the worst way possible. The EHO framework or initiatives were shown as follows [20].

**Step 1:** Initialization Process.

These procedures set the hidden layers, neurones, basis weights (which range from  $-10$  to  $+10$ ), and reference values for the RNN using real learning function values. The EHO parameters are scaling factors and the optimisation model starts with random values.

**Step 2:** Process for Evaluating Fitness.

The weak soil formation and EHO settling are taken into consideration by this Geogrid model. Below is the equation that is produced when this value is derived utilising the best hidden layers and RNN structure neurones.

$$FF = \delta \tag{10}$$

Utilizing the hybrid algorithm, the fitness is attained.

**Step 3:** Current elephant location.

The best and worst options for each elephant in each family in this third stage, with the exception of the matriarch and a male elephant, are included in the status of each elephant  $P$  and each clan  $C_i$  has elephants. The elephant's  $i = 1, 2, 3, \dots, P$  rank and  $j^{\text{th}}$  clan  $i = 1, 2, 3, \dots, C$  are symbolised by  $L_{c_{i,j}}$ . The elephant's current location  $i^{\text{th}}$  is stated as,

$$L_{new,c_{i,j}} = L_{c_{i,j}} + \alpha(L_{best,c_{i,j}} - L_{c_{i,j}}) * r \tag{11}$$

Here  $L_{new,c_{i,j}}$  is the updated position,  $L_{c_{i,j}}$  is the old position,  $L_{best,c_{i,j}}$  is the Position of best in the clan.  $\alpha$  and  $\beta = 0$  to 1.

By following the methods above, the optimum position that reflects the matriarch cannot be modified.

**Step 4:** Movement update for each clan's fittest elephant.

The position update for the clan member that fits in best is provided by,

$$L_{new,c_{i,j}} = \beta * L_{center,c_j} \text{ and } L_{center,c_i} = \sum_{i=1}^n \frac{L_{c_{i,j}}}{n_l} \tag{12}$$

Here  $n_l$  the overall quantity of elephants in individually clan and  $\beta \in \{0, 1\}$

**Step 5:** Separating the worst of the clan's elephants.

Male elephants or the worst elephants would be taken away from their family groupings. The lowest ranking changed to,

$$L_{worst,c_{i,j}} = L_{min} + (L_{max} - L_{min} + 1) * r \tag{13}$$

where  $L_{worst,c_{i,j}}$  is the clan's worst male elephants,  $L_{max}$  and  $L_{min}$  are, as well as the elephants' permitted maximum and lowest range.

**Step 6:** Ending procedure.

It completes one iteration since the weakest elephant in the clan has been separated. The process is continued until the RNN's leaning function for settling weak soil formation is achieved, at which time it is deemed complete. Steps 2 through 6 are repeated until the convergence requirements are met if the criteria are not met. The process flow diagram for the hybrid RNN-EHO technique is shown in Fig. 3.



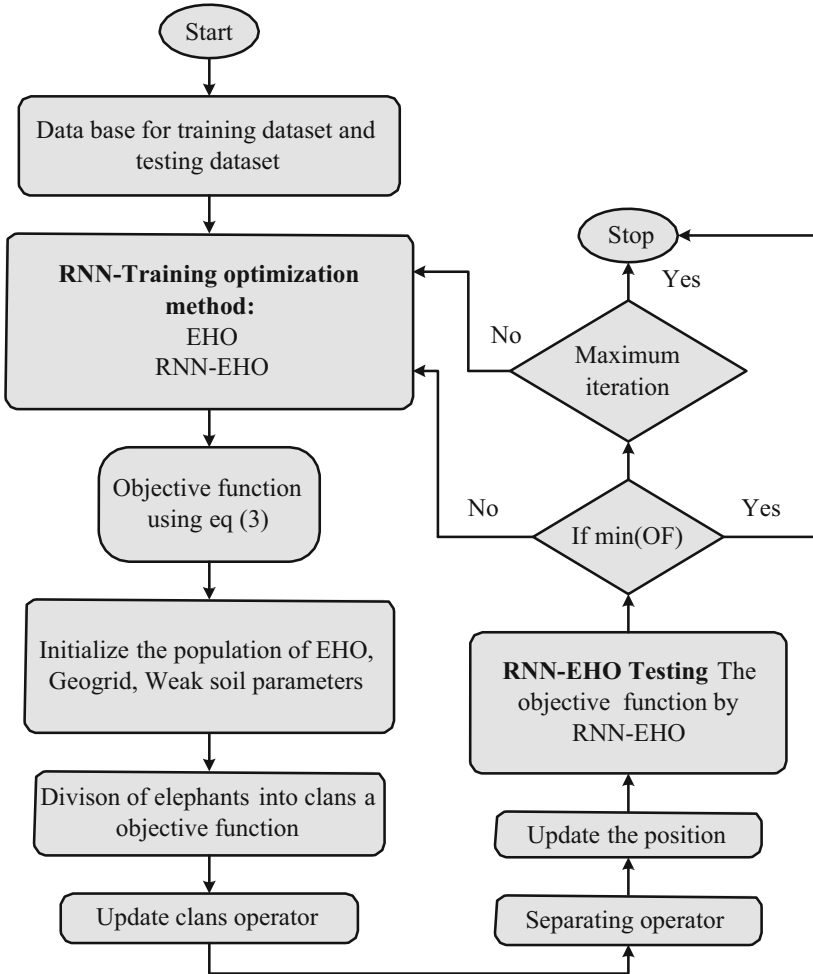


Fig. 3. Flowchart of proposed hybrid RNN-EHO method

### 3 Results and Discussion

Two reinforced and unreinforced examples with the test results are provided. It will be explained how bearing pressure compares to normalised settlement, how much of the load is supported by piles, and how axial stress is distributed throughout the length of the pile. The ideal cushion thickness and pile spacing were found in the unreinforced case, while in the reinforced case, the ideal placement of the first layer of the geogrid and the ideal length of geogrids were discovered. The Geogrid sand foundations are powered by Matlab 7.10.0 (R2021a) and an Intel (R) Core (TM) i5 CPU with 4GB RAM. In order to confirm its performance, the new system was put to the test and its processing parameters were compared to a number of techniques, including the Artificial Neural

Network (ANN), Harris Hawks Optimization (HHO), Cuttlefish algorithm (CFA), and Mayfly Optimization Algorithm (MOA) models.

### 3.1 Uncertainty Analysis

Wilmot’s Index of Agreement (WI), Mean Absolute Percentage Error (MAPE), Mean Absolute Percentage Error (RMSE), Mean Absolute Percentage Error (MAPE), Mean Absolute Percentage Error (RMSE), coefficient of correlation ( $R^2$ ), and mean absolute error (MAE) were all calculated to evaluate the performance of the final selected architecture for the proposed ANN-MGSA (i.e., testing information that the network hasn’t encountered throughout the training process). Equations (14) to (18) are used to compute the values of MAE (mean absolute error), RMSE (root-mean-square error), and R for the training and testing portions.

Five indicators were used to assess how well the suggested machine learning models performed:

**RMSE:** The standard errors between predicted values and actual values can be represented using RMSE. The algorithm is defined as being given in Eq. (14) and is said to be more exact the smaller the RMSE.

$$RMSE = \sqrt{\frac{1}{n} \sum_{i=1}^n (O_s^i - P_s^i)^2} \tag{14}$$

**Correlation Coefficient (R):**  $R$  Measures how strongly the measured values and the variation in forecasted values are related. The  $R$  value varies from  $-1$  to  $1$ , where  $-1$  denotes a completely inverse correlation and  $1$  denotes a completely inverse correlation. The definition of  $R$  is given in Eq. (15)

$$R(p^i, O^i) = \frac{cov(p^i, O^i)}{\sqrt{var[p^i] * var[O^i]}} \tag{15}$$

**Mean Absolute Percentage Error (MAPE):** A dimensionless measure called MAPE may be used to rate a model’s ability to anticipate outcomes. The greater the model’s derived predictive performance, the closer MAPE is to 0. Equation represents the MAPE definition (16).

$$MPA = \frac{100\%}{n} \sum_{i=1}^n \frac{|P_s^i - O_s^i|}{P_s^i} \tag{16}$$

**Coefficient of Determination ( $R^2$ ):**  $R^2$  measures how closely the anticipated value resembles the actual value.  $R^2$  is between 0 and 1. The perfect match between the anticipated value and the actual value is shown by an  $R^2$  of 1. Equation (17) displays  $R^2$ ’s definition.

$$R^2 = 1 - \frac{\sum_{i=1}^n |P_s^i - O_s^i|}{\sum_{i=1}^n |O_s^i - O_s|} \tag{17}$$

**Wilmot’s Index of Agreement (WI):** WI, which ranges from 0 to 1, is a standardised index to measure the prediction efficacy of established models. A WI of 0 shows no match at all, whereas a WI of 1 shows complete agreement between predicted values and actual values. Equation (18) displays the WI definition.

$$WI = 1 - \frac{\sum_{i=1}^n |P_S^i - O_S^i|}{\sum_{i=1}^n |O_S^i - O_S^i|} \tag{18}$$

where,  $O_S^i$ ,  $P_S^i$  and  $n$  stands for  $i^{th}$  the observed value of settlement,  $i^{th}$  the anticipated value of settlement, and the quantity of data samples, respectively (Table 2) (Fig. 4).

**Table 2.** Analysis of suggested models and other approaches based on statistical indices for comparison

Statistical index	ANN	HHO	CFA	MOA	Proposed
RMSE	0.813	0.586	0.512	0.481	0.352
MAE	0.44	0.321	0.28	0.26	0.22
Efficiency	0.963	0.974	0.977	0.98	0.985
RWI	0.897	0.885	0.905	0.933	0.951

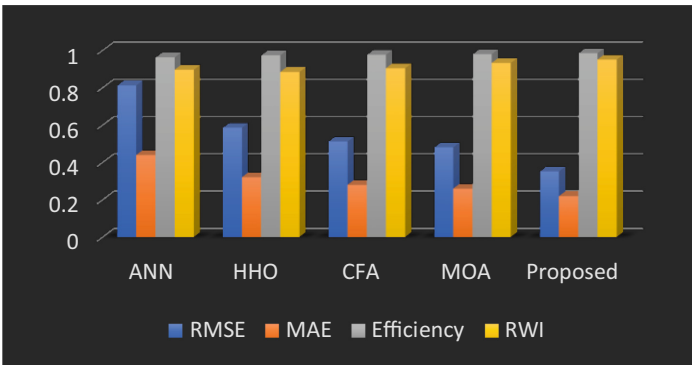


**Fig. 4.** Performance analysis of statistical measurement

Three different scenarios’ pressure-settlement behaviours are compared in Fig. 5. The bearing capacity of the geogrid reinforced foundation bed increased with the height of the geogrid. Comparable observational methods that rely on numerical analysis. As the geocell’s height increases, the footing load will be dispersed across a larger area. Figure 6 illustrates typical data on settlement variation for a 53 mm thick granular subbase layer with various geosynthetic reinforcement layer types. The results demonstrated that the initial modulus of the poor sand is relatively high; as settlement increased with the number of cycles, the modulus value decreased; and ultimately, near the conclusion of

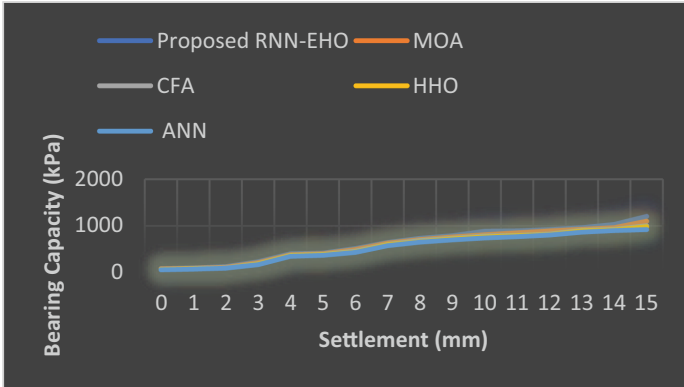


**Fig. 5.** Comparative analysis of Pressure–settlement performed on 150 mm thick granular subbase layer

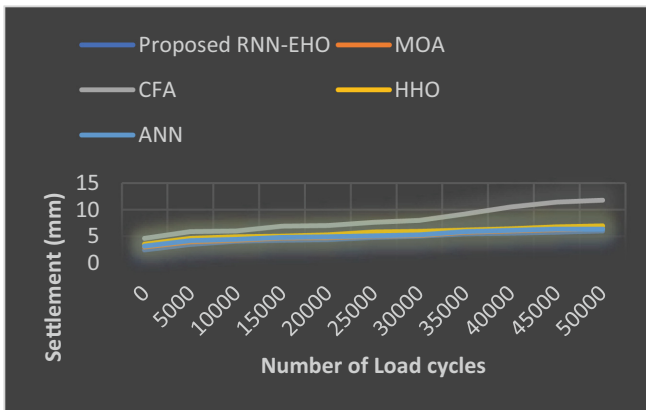


**Fig. 6.** Results of settlement with number of load repetitions

22000 cycles, the modulus value stabilised at a constant value. Figure 7 shows that with geogrid of an 80 mm height, the ultimate bearing capacity of lime stone aggregate bases reinforced with geogrid increases by 1.1 times over unreinforced bases. Additionally, a 76 percent increase in the total bearing capacity augmentation factor was made. The findings show a significant increase in the performance of the suggested RNN-EHO approach employing Geogrid compared to other techniques such as ANN, CFA, MOA, and HHO, respectively, when the proposed method course was correctly compacted.

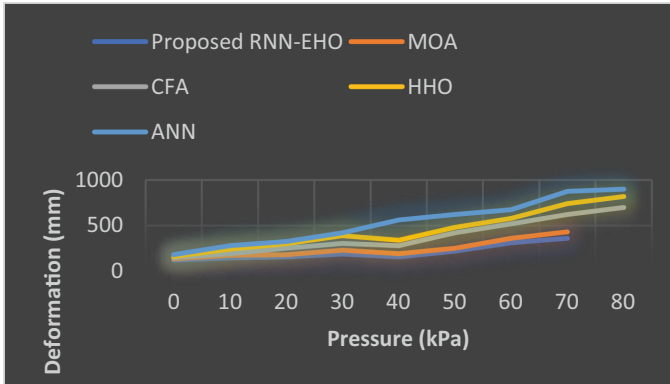


**Fig. 7.** Showing comparison of deformation of exiting methods and proposed method at the centre with 120 mm thick base

## 4 Conclusion

Analyses and pertinent conclusions were reached by applying the geogrid to the precise geometry of a ballasted railway track substructure utilizing a proven recommended hybrid RNN-EHO technique. It may be possible to analyze the system's performance on actual railroads using realistic geometry and applications. The assessments mimicked weaker track material, compressible subgrades, and the impacts of reinforcing material on overall performance by varying the stiffness of the foundation, the geogrid, and the ballast. In this report, a hybrid recurrent neural network (RNN)-elephant herding optimization (EHO) technique was introduced to investigate the geogrid-reinforced sand's improvement under static stress. The containment of the ballast using geogrid was particularly efficient in decreasing vertical deformations, even when low-quality material was utilized, according to numerical modeling of geogrid applied to a railway scenario.

- Although geogrid confinement was used, the reduction in vertical settlement was not as substantial as anticipated. This is promising since it could allow for longer maintenance cycles when the ballast loses shear strength or the use of weaker ballast materials, including recycled ballast or well-graded particles.
- The likely cause of this is because the subgrade is subject to significant forces whether or not there is a geogrid. The geogrid did help with the loads being distributed more uniformly, which may have prevented the development of significant shear stresses and collapse, particularly on softer subgrades. The geogrid reduces vertical settling on stronger foundations by lessening the lateral ballast pressure brought on by heavy loads.

## References

1. Nguyen, V.D., et al.: Monitoring of an instrumented geosynthetic-reinforced piled embankment with a triangular pile configuration. *Int. J. Rail Transp.* 1–23 (2022)

2. Schary, Y.: Case studies on geocell-based reinforced roads, railways and ports. In: Sitharam, T.G., Hegde, A.M., Kolathayar, S. (eds.) *Geocells*. STCEE, pp. 387–411. Springer, Singapore (2020). [https://doi.org/10.1007/978-981-15-6095-8\\_15](https://doi.org/10.1007/978-981-15-6095-8_15)
3. Deshpande, T.D., et al.: Analysis of railway embankment supported with geosynthetic-encased stone columns in soft clays: a case study. *Int. J. Geosyn. Ground Eng.* **7**(2), 1–16 (2021). <https://doi.org/10.1007/s40891-021-00288-5>
4. Lazorenko, G., et al.: Failure analysis of widened railway embankment with different reinforcing measures under heavy axle loads: A comparative FEM study. *Transp. Eng.* **2**, 100028 (2020)
5. Sweta, K., Hussaini, S.K.K.: Effect of geogrid on deformation response and resilient modulus of railroad ballast under cyclic loading. *Constr. Build. Mater.* **264**, 120690 (2020)
6. Hubballi, R.M.: Stabilization of railway tracks using geosynthetics—a review. In: Dey, A.K., Mandal, J.J., Manna, B. (eds.) *Proceedings of the 7th Indian Young Geotechnical Engineers Conference*. LNCE, vol. 195, pp. 387–396. Springer, Singapore (2022). [https://doi.org/10.1007/978-981-16-6456-4\\_40](https://doi.org/10.1007/978-981-16-6456-4_40)
7. Banerjee, L., Chawla, S., Dash, S.K.: Application of geocell reinforced coal mine overburden waste as subballast in railway tracks on weak subgrade. *Constr. Build. Mater.* **265**, 120774 (2020)
8. Meena, N.K., et al.: Effects of soil arching on behavior of pile-supported railway embankment: 2D FEM approach. *Comput. Geotechn.* **123**, 103601 (2020)
9. Jain, S.K., Saleh Nusari, M., Acharya, I.P.: Use of geo-grid reinforcement and stone column for strengthening of mat foundation base. In: *Proceedings of Materials Today* (2020)
10. Mei, Y., et al.: Experimental study of the comprehensive technology of grouting and suspension under an operating railway in the cobble stratum. *Transp. Geotechn.* **30**, 100612 (2021)
11. Ziegler, M.: Application of geogrid reinforced constructions: history, recent and future developments. *Procedia Eng.* **172**, 42–51 (2017)
12. Yu, Z., et al.: True triaxial testing of geogrid for high speed railways. *Transp. Geotechn.* **20**, 100247 (2019)
13. Esmaeili, M., et al.: Investigating the effect of geogrid on stabilization of high railway embankments. *Soils Found.* **58**(2), 319–332 (2018)
14. Zhang, C., Su, L., Jiang, G.: Full-scale model tests of load transfer in geogrid-reinforced and floating pile-supported embankments. *Geotext. Geomembr.* **50**, 869–909 (2022)
15. Punetha, P., Nimbalkar, S.: Performance improvement of ballasted railway tracks for high-speed rail operations. In: Barla, M., Di Donna, A., Sterpi, D. (eds.) *Challenges and Innovations in Geomechanics*. LNCE, vol. 126, pp. 841–849. Springer, Cham (2021). [https://doi.org/10.1007/978-3-030-64518-2\\_100](https://doi.org/10.1007/978-3-030-64518-2_100)
16. Esen, A.F., et al.: Stress distribution in reinforced railway structures. *Transp. Geotechn.* **32**, 100699 (2022)
17. Watanabe, K., et al.: Construction and field measurement of high-speed railway test embankment built on Indian expansive soil “Black Cotton Soil.” *Soils Found.* **61**(1), 218–238 (2021). <https://doi.org/10.1016/j.sandf.2020.08.008>
18. Bonatti, C., Mohr, D.: On the importance of self-consistency in recurrent neural network models representing elasto-plastic solids. *J. Mech. Phys. Solids* **158**, 104697 (2022)
19. Li, W., Wang, G.-G.: Elephant herding optimization using dynamic topology and biogeography-based optimization based on learning for numerical optimization. *Eng. Comput.* **38**(2), 1585–1613 (2021). <https://doi.org/10.1007/s00366-021-01293-y>
20. Guptha, N.S., Balamurugan, V., Megharaj, G., Sattar, K.N.A., DhiviyaRose, J.: Cross lingual handwritten character recognition using long short term memory network with aid of elephant herding optimization algorithm. *Pattern Recogn. Lett.* **159**, 16–22 (2022). <https://doi.org/10.1016/j.patrec.2022.04.038>